Ecological Indicators 147 (2023) 109930

Contents lists available at ScienceDirect

Ecological Indicators

journal homepage: www.elsevier.com/locate/ecolind

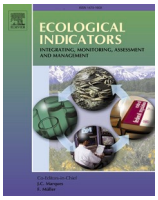

# Growth and carbon sequestration of poplar plantations on the Tibetan Plateau

Yuan Yao [a,1], Shumiao Shu [b,1], Wenzhi Wang [b], Ruixuan Liu [a], Yuelin Wang [c], Xiaodan Wang [b,*], Sheng Zhang [a,*]

[a] Key Laboratory for Bio-resources and Eco-environment of the Ministry of Education, College of Life Sciences, Sichuan University, Chengdu 610065, China
[b] Key Laboratory of Mountain Surface Processes and Ecological Regulation, Institute of Mountain Hazards and Environment, Chinese Academy of Sciences, Chengdu 610299, China
[c] College of Tourism and Urban-Rural Planning, Chengdu University of Technology, Chengdu 610059, China

ARTICLE INFO

*Keywords:*
*Populus*
Iterative growth model
Tree ring
Low-frequency growth signals
Yarlung Tsangpo River

ABSTRACT

Tree radial growth has long-term adaptation and rapid responses to climate, manifested as age-dependent low-frequency and climate-sensitive high-frequency signals. Although the former is usually removed in climate-growth analyses, its overall change still profoundly affects forest biomass and carbon sequestration. The iterative growth model (IGM) reveals the underlying links among organism lifespan, growth rate, and respiration, providing a set of theoretical indicators to evaluate or predict growth. Here, IGM was extended to the tree-ring scale (IGMR) to study the low-frequency growth signals of poplar plantations in the Yarlung Tsangpo River, Tibetan Plateau. As predicted by the IGMR, the low-frequency growth signals all follow a unimodal pattern over the diameter at breast height (DBH) gradient while constraining the high-frequency signals. The unimodal growth curves' length (maximum DBH), height (maximum growth rate of tree DBH), and resulting tree lifespan could be used to assess and predict tree growth. The results showed that the maximum DBH, growth rate and inverse of the longevity of the trees were greater at lower elevations. The indicators of *Populus* × *beijingensis* (PB) were better than those of *P. alba* (PA). Overall, poplars adapted to the plateau climate by reducing growth rates and increasing longevity. Temperature was the key factor affecting these trade-offs, with the best temperature at 14.69 ℃. Combined with stand density, PB plantations (11695.58 ± 1704.98 g/m$^2$) had greater potential maximum biomass than PA plantations (9032.50 ± 2031.21 g/m$^2$). This study highlights that the response of low-frequency growth signals to environments is holistic, and the resulting indicators have important value for evaluating and predicting tree growth and forest carbon sequestration. Moreover, the results have important practical significance for reasonable plantations and proper assessment of the ecological contribution of plantation forests on the Tibetan Plateau.

*Abbreviations:* *b*, metabolic exponent; *d*, forest density; *D*, average *f(m)*; DBH, diameter at breast height; *D/T*, organism/tree mean growth rate; *f*(m), the total biomass of new tissue created during the formation time; *f(m)/T*, the growth rate; *o*, the initial biomass; *f(r)*, the increment in *r* during time *T*; $g_r$, cost of respiration needed to produce a unit of tissue; HPA, high altitude of PA plantations; HPB, high altitude of PB plantations; IGM, iterative growth model; IGMF, IGM expansion at the forest scale; IGMF-L, the thermodynamic lower boundaries of forest NPP; IGMF-U, the thermodynamic upper boundaries of forest NPP; IGMR, tree-ring iterative growth model; IGMR-L, the thermodynamic lower boundaries of tree ring growth; IGMR-U, the thermodynamic upper boundaries of tree ring growth; LPA, low altitude of PA plantations; LPB, low altitude of PB plantations; *m*, organism/tree current size; *M*, organism/tree potential maximum size; $m_r$, rate of maintenance respiration per unit of tissue; MPA, middle altitude of PA plantations; MPB, middle altitude of PB plantations; NPP, net primary productivity; PA, *Populus alba* L; PB, *Populus* × *beijingensis*; *r*, current tree DBH; $r_0$, the initial DBH; *R*, the maximum DBH; *T*, formation time of unit tissue, which is primarily controlled genetically and by physiological activities, with the intrinsic or developmental growth rate independent of organism size; *X*, forest current biomass; $X_{max}$, forest potential maximum biomass.

* Corresponding authors.
*E-mail addresses:* wxd@imde.ac.cn (X. Wang), shengzhang@scu.edu.cn (S. Zhang).
[1] These authors contributed equally.

https://doi.org/10.1016/j.ecolind.2023.109930
Received 24 October 2022; Received in revised form 28 December 2022; Accepted 13 January 2023
Available online 23 January 2023

## 1. Introduction

Tree growth drives forest carbon sequestration, offsetting 25% of yearly anthropogenic carbon emissions and thus positively mitigating climate change (Cabon et al., 2022; Locosselli et al., 2020). Tree radial growth is an important indicator of tree growth, recording climate change and tree intrinsic growth trends. The intrinsic growth trend follows the unimodal curve on the age or size (DBH) gradient. Although specific size-dependent patterns are related to climate, competition, and functional traits (Herault et al., 2011), they are usually considered separately from climate-sensitive high-frequency signals. This knowledge is mainly derived from the stationarity assumption or uniformity principle, manifesting as a robust, consistent relationship between ring width and climate after removing "age effects." However, over longer time windows, especially for forests experiencing new global climate events (Overpeck, 2013; Sobel et al., 2016; Richardson et al., 2018), the uniformity principle could change with the tree's physiological status (Peltier and Ogle, 2020). How climate drives terrestrial net primary production (NPP) remains controversial in the global ecology. Specifically, whether climate directly affects plant physiological processes and thus influences NPP or indirectly by constraining forest biomass, tree age structure, and growing season length. Recent studies suggested that the "direct" effect may be equivalent to its "indirect" effect (Michaletz et al., 2017). Changes in low-frequency growth signals could cause different growth-climate sensitivities and have a more profound impact on forest carbon sequestration.

To our knowledge, the kinetic mechanism of low-frequency growth signals and their response to climate is still unknown. Some studies have suggested that this signal follows a clear hump-shaped pattern related to functional traits and size (Herault et al., 2011; Matsushita et al., 2015; Shi et al., 2013). Recent global results further showed an inherent trade-off in tree-ring growth rate and lifespan (Brienen et al., 2020; Locosselli et al., 2020), implying overall changes in the unimodal curve. Tree respiration concerns the transport, release, and use of energy to grow, maintain and defend tree life, where energy-demanding processes also follow the first and second laws of thermodynamics and the allometric scaling laws of metabolism. Based on metabolic growth theory and these details, Shu et al. (2021) derived a complete organism growth model known as the iterative growth model (IGM). However, individual biomass parameters in this model are often difficult to obtain directly, especially for trees. Such limitations make it difficult to directly reveal the tree growth pattern through the model. Here, based on the scaling relationship between tree biomass and tree DBH (West et al., 1999), the IGM was first extended to the tree ring scale to determine the low-frequency tree-ring signals. Then the critical indicators of tree growth were obtained: the tree's maximum DBH, lifespan, and the mean (or maximum) growth rate of tree DBH. The ecological adaptability of trees and estimation of the potential forest biomass could be assessed after combining the stand density based on these indicators.

China has been working to protect the fragile ecological function of the Tibetan Plateau through afforestation, especially in the Yarlung Tsangpo River basin (Liu et al., 2020; Ma et al., 2020; Zhang et al., 2018). Poplars (*Populus* × *beijingensis* (PB) and *P. alba* L (PA)) have long been the main afforestation species in this area because of their fast growth and strong ecological adaptability (Debeljak et al., 2014; Hajima et al., 2014; He et al., 2021; Liao et al., 2020; Lu et al., 2013). Although the area of afforestation in Tibet is expanding, its single species and structure are more vulnerable to climate change than those of natural forests (Camarero et al., 2021; Navarro-Cerrillo et al., 2020; Santini et al., 2020). In this context, the growth trends of plantations are still unknown, which can profoundly affect potential forest carbon sequestration. Here, the poplar growth trends behind their low-frequency tree-ring signals were first determined using the extension of IGM. Then, these trends were linked to forest carbon sequestration dynamics. This work aimed to reveal the growth trends of poplars and the possible potential carbon sequestration of poplar plantations in the Yarlung Tsangpo River basin with different elevational distributions.

## 2. Materials and methods

### 2.1. Study area

The study area was located in the Yarlung Tsangpo River basin of the South Tibetan Plateau. It has a plateau semiarid monsoon climate: the annual mean temperature is 5.92 ℃, and the annual mean precipitation is 428.70 mm (Li et al., 2013; Liu et al., 2018). The terrain exhibits high elevation in the west and low elevation in the east (Fig. 1**A**). Poplars are mainly used for afforestation projects in this area and are widely planted on riverbanks (Fig. 1**B**). Among the poplar species, PB and PA were the largest planting species. In April 2021, three elevation gradients from 2880 m to 3830 m were established in the Yarlung Tsangpo River basin: ~ 3200 m for low, ~ 3500 m for middle, and ~ 3700 m for high elevation sites (Table 1).

Moreover, 14 large poplar plantation sites were selected, including six sampling sites (PB3, PB5, PB8, PA1, PA3, and PA6) and eight survey sites (PB1, PB2, PB4, PB6, PB7, PA2, PA4, and PA5) (Fig. 1**A and** Table 1). The longitude and latitude of the sites were between 29°02′-29° 49′ N and 88° 50′-93° 39′ E (Fig. 1**A and** Table 1). The sampling sites were mainly used to collect tree core samples and investigate stand density and DBH. Meanwhile, the survey sites were mainly used for measuring DBH. At each site, a quadrat was established (approximately 400 $m^2$) for sampling and surveying.

### 2.2. Sample collection and experimental analysis

At each sampling quadrat, two cores from every living tree at breast height (1.3 m) were sampled on the basis of cross-intersect method using diameter borers (Ling et al., 2017). These tree core samples were taken to the laboratory to measure the ring widths by using the LINTAB ring-width measurement system (Rinntech, Heidelberg, Germany), with a precision of 0.001 mm after air-drying and sanding each core until the tree ring boundaries were clearly visible. As poplar belongs to diffuse-porous species, many core samples with unclear demarcated annual rings were abandoned. After all sample measurements were completed, the COFECHA program (a software package) was used to check the results and confirm the cross-dating accuracy (Holmes, 1983), and then the standard chronologies were established using ARSTAN (another software package).

### 2.3. Acquisition of meteorological and NPP data

Climatic data were collected from the three meteorological stations with different elevation distributions and nearest to the sampling sites (NOAA - National Centers for Environmental Information, https://www.ncei.noaa.gov). Nyingchi (29° 57′ N, 94° 47′ E, 3001 m), Lhasa (29° 67′ N, 91° 13′ E, 3650 m), and Shigatse weather stations (29° 25′ N, 88° 88′ E, 3837 m) (Fig. 1**A**). The meteorological data spanned from 1980 to 2020. The data from these sites (mean annual temperature and mean annual precipitation) were used to analyze the effects of climate factors on growth-lifespan trade-offs and predict their optimal outcomes. In addition, monthly climate factors (mean monthly temperature and monthly total precipitation) were used to obtain plantation responses to climate change. The annual NPP data were collected from the Beijing Normal University Data Center (Liang et al., 2021) to verify the correctness of the IGM for forest NPP (**Eq. (6)**) and estimate the stands' current and potential maximum biomasses at the survey sites.

### 2.4. IGM and its extensions

Based on the allometric scaling laws of metabolism, the IGM provides a general kinetic framework for organism growth. Compared with other metabolic growth models (*i.e.*, the ontogenetic growth model), it has two

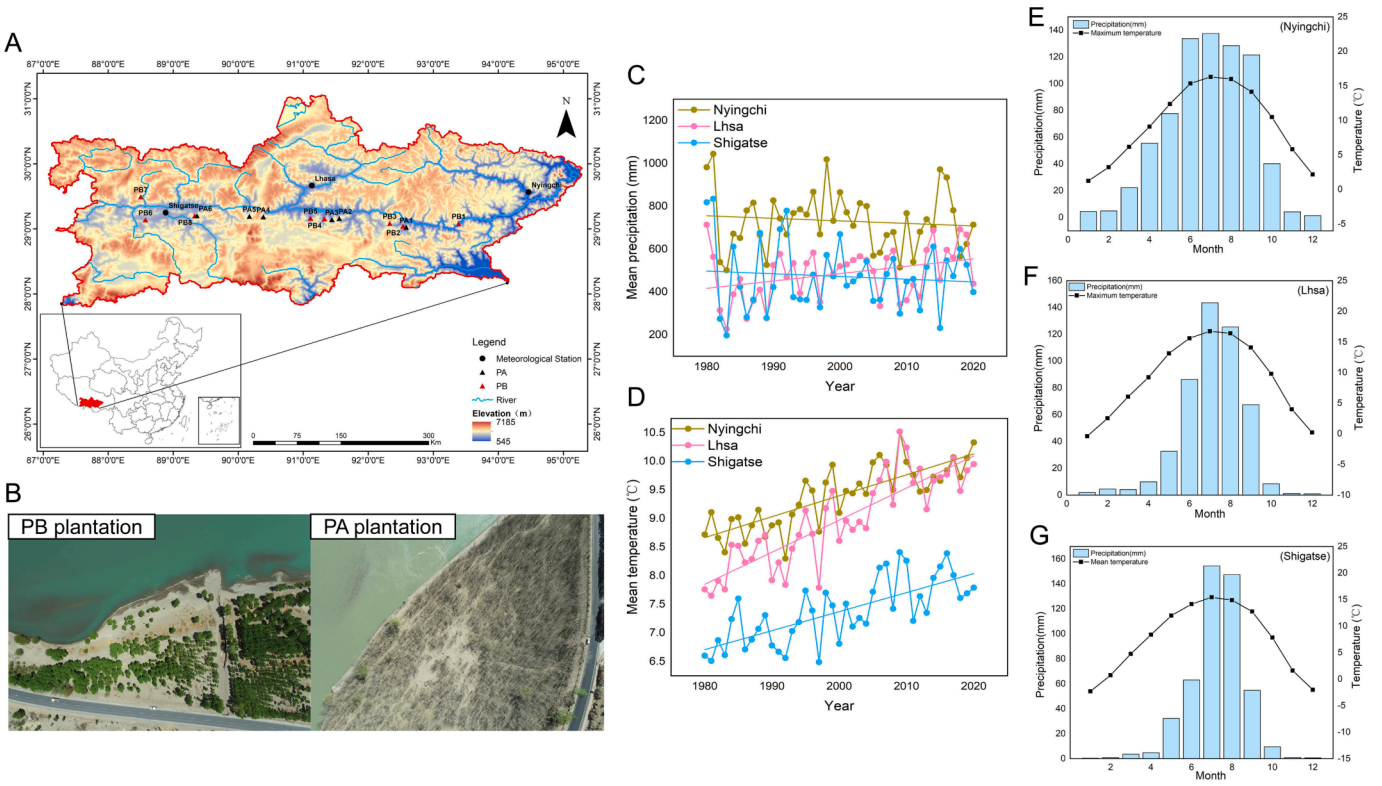


**Fig. 1.** Map of the research area and climate elements in the Yarlung Tsangpo River basin, Tibetan Plateau. (A) Locations of sampling sites, survey sites, and nearest meteorological stations. (B) Aerial image of poplar plantation in the Yarlung Tsangpo River basin. (C) Annual mean precipitation from 1980 to 2020. (D) Annual mean temperature from 1980 to 2020. (E) Monthly mean temperature and monthly total precipitation of the Nyingchi weather stations. (F) Monthly mean temperature and monthly total precipitation of the Lhasa weather stations. (G) Monthly mean temperature and monthly total precipitation of the Shigatse weather stations.

**Table 1**
Geographic description of the sampling and survey sites.

| Tree species | Site code | Type of site | Latitude | Longitude | Altitude (m) | Landform | Soil texture | Mean stand DBH (cm) | Mean stand density (stems/ ha) |
|---|---|---|---|---|---|---|---|---|---|
| | PB1 | survey | 29.08 | 93.39 | 2880 (L) | terrace | sandy soil | 32.07 | / |
| | PB2 | survey | 29.04 | 92.53 | 3080 (L) | terrace | sandy soil | 27.17 | / |
| | PB3 | sampling | 29.09 | 92.33 | 3160 (L) | terrace | sandy soil | 27.84 | 422 |
| | PB4 | survey | 29.16 | 91.33 | 3540 (M) | terrace | sandy soil | 28.92 | / |
| PB | PB5 | sampling | 29.16 | 91.11 | 3560 (M) | terrace | sandy soil | 30.94 | 367 |
| | PB6 | survey | 29.14 | 88.57 | 3830 (H) | terrace | sandy soil | 23.54 | / |
| | PB7 | survey | 29.49 | 88.50 | 3830 (H) | terrace | sandy soil | 19.54 | / |
| | PB8 | sampling | 29.20 | 89.33 | 3750 (H) | terrace | sandy soil | 16.16 | 511 |
| | PA1 | sampling | 29.02 | 92.59 | 3140 (L) | terrace | sandy soil | 29.18 | 434 |
| PA | PA2 | survey | 29.16 | 91.55 | 3560 (M) | terrace | sandy soil | 11.41 | / |
| | PA3 | sampling | 29.15 | 91.44 | 3530 (M) | terrace | sandy soil | 17.55 | 522 |
| | PA4 | survey | 29.19 | 90.39 | 3590 (M) | terrace | sandy soil | 15.66 | / |
| | PA5 | survey | 29.19 | 90.17 | 3710 (H) | terrace | sandy soil | 21.34 | / |
| | PA6 | sampling | 29.20 | 89.36 | 3770 (H) | terrace | sandy soil | 14.42 | 488 |

Abbreviations: L: low elevation sites, M: middle elevation sites, H: high elevation sites.

improvements. First, the formation time of a unit of tissue ($T$) was introduced. Second, the metabolic scaling exponent ($b$) equal to 0.75 was eliminated. Thus, a basic and flexible discrete growth equation could be derived (Mori et al., 2010; Shu et al., 2021).

$$\frac{f(m)}{T} = \frac{m_r}{g_r}\left(M^{1-b}m^b - m\right) \quad (1)$$

where $f$(m) is the total biomass of new tissue created during time $T$, $f(m)/T$ represents the growth rate, $M$ and $m$ are the maximum biomass and current biomass of organisms, respectively, and $g_r$ and $m_r$ are the cost of respiration needed to produce a unit of tissue and the rate of maintenance respiration per unit of tissue, respectively. Usually, $g_r$ is stable, ranging from 0.2 to 0.4, and we used 0.33 in this study (Cannell and Thornley, 2000; Gower et al., 1997; Piao et al., 2010; Thornley and Cannell, 2000; Thornley, 2011). Meanwhile, $m_r$ is sensitive to the environment and is mainly driven by temperature following the Arrhenius equation (Amthor, 2000; Clarke, 2019; Piao et al., 2010; Shu et al., 2019; Shu et al., 2021). The IGM contains some implicit theoretical and mathematical constraints. The first constraint is $T < g_r/m_r$, derived from the thermodynamic significance of respiration (Shu et al., 2021). Second, from a mathematical perspective, $M$ maintains a strict mathematical relationship with other parameters as follows (Shu et al.,

2021):

$$M = \frac{D}{T}\frac{g_r}{m_r}\frac{2b+2}{1-b} \quad (2)$$

where $D$ is the average $f(m)$, mainly determined by the ability of plants to absorb resources and the supply of resources, and $TM/D$ or $g_r/m_r \times (2b + 2)/(1\text{-}b)$ represents the total growth time. The ground for this equation is an integral transform from $f(m)$ to $M$ (Shu et al., 2021).

The IGM is also valid for tree-ring dynamics by the scaling relationship between tree biomass ($m$) and tree DBH ($r$), which could be expressed as follows (West et al., 1999):

$$r \propto m^{b/2} \quad (3)$$

Combining Eqs. (3) and (1) yields the following expression:

$$f(r) = \left(T\frac{m_r}{g_r}(r-r_0)^{2/b}\left(\left(\frac{R}{(r-r_0)}\right)^{2/b-2} - 1\right) + (r-r_0)^{2/b}\right)^{b/2} - r + r_0 \quad (4)$$

where

$f(r)$ is the increment in r during time $T$;

$r_0$ is the initial DBH;

$R$ is the maximum DBH;

$b$ is usually taken as 0.75 for trees (Mori et al., 2010).

When $T \to 0$ and $g_r/m_r$, Eq. (4), could be simplified as follows:

$$o(r) = \frac{b}{2}\frac{m_r}{g_r}\left(R^{2/b-2}(r-r_0)^{3-2/b} - r + r_0\right) \quad (5a)$$

$$o(r) = \frac{m_r}{g_r}\left(R^{1-b}(r-r_0)^b - r + r_0\right) \quad (5b)$$

where

$o(r)$ is the growth rate of tree DBH, *i.e.*, $f(r)/T$. (approximately equal to twofold of the tree-ring growth rate).

Mathematically, Eq. (4) is between Eqs. (5a) and (5b). Eq. (4) was termed the iterative growth model in tree-ring growth (IGMR), and Eqs. (5a) and Eq. (5b) were denoted as the thermodynamic lower (IGMR-L) and upper (IGMR-U) boundaries of tree ring growth. In addition, observations showed that when trees attain their potential maximum size, their mortality increases significantly. Therefore, the maximum growth time was assumed to be equivalent to the lifespan (Brienen et al., 2020; Johnson et al., 2018).

Due to the density effects, Eq. (1) could also be extended to the forest scale, where the relationship between tree DBH and forest NPP could be expressed as follows (for specific derivation, see supplementary information):

$$NPP = X\frac{m_r}{g_r}\left(c\left(\frac{R}{r}\right)^{2/3} - 1\right) \quad (6)$$

where

$c$ is a turnover-related parameter equal to 1.15 for aboveground NPP (see supplementary information);

X is the forest's current biomass (converted to grams of C assuming biomass is 47% carbon, same as below) (Ipcc, 2006).

In addition, the ratio of the forest's potential maximum biomass ($X_{max}$) to $X$ is equal to $(R/r)^{2/3}$.

Using regional and global data, the validity of the IGMR and IGMF (IGM expansion at the forest scale) was confirmed. Here, a set of tree-ring data was used to test the IGMR. These data were collected from a primary *Abies fabri* forest over 150 years old and located in Gongga Mountain on the southeastern Tibetan Plateau (data from Wang et al., 2017). The IGMR could explain the growth-DBH relationship well. The primary forest's mean growth rate of tree DBH showed a clear single-peaked pattern in DBH gradients (Fig. S1A). Moreover, IGMF could explain the large variation in aboveground NPP across broad environmental gradients (Fig. S1**B**). The data set includes over 1,200 woody plant communities across broad climate gradients (mainly distributed in China) (data from Michaletz et al., 2014). In addition, the total growth time estimated by IGMF was slightly lower than the negative power-exponential curve relationship between mean annual temperature and tree longevity and was within the 95% confidence interval of the actual curve at both biome scales (data from Locosselli et al., 2020) (Fig. S1**C**).

### 2.5. Calculation of biomass and carbon stocks

For sampling sites, the stand DBH dynamics were obtained from the stand mean DBH and annual mean tree-ring width increments. The aboveground biomass dynamics of individual poplars were calculated by the tree biomass equation and DBH dynamics (Guan and Liu, 1993) (Table 2). The stand aboveground biomass was calculated from the product of the individual poplar biomass and the density (Tables 1 and 2). The carbon stock was calculated from the biomass and the carbon content rate. The aboveground NPP was calculated based on the IGM for forest NPP (**Eq. (6)**) and stand aboveground carbon stock, assuming that the plantation density was constant for a decade. Linear regression analyses verified the correctness of the IGM for forest NPP.

After verification was conducted, the maximum DBH and $m_r/g_r$ value of the same poplar species at the same elevation gradient were assumed to be the same. The stand current and potential maximum biomass of survey sites were also calculated by using the current mean stand DBH, NPP data, IGM for forest NPP, and the relationship between forest mean DBH and biomass (*i.e.*, $(R/r)^{2/3} = X_{max}/X$, see supplementary information).

### 2.6. Statistical analysis

Statistical analyses were conducted using SPSS 26.0 (SPSS Inc., IL, USA). The differences in biomass and carbon stock were tested using the Kruskal-Wallis test. The diagram and linear regression analyses were performed using Origin 2018 (Origin Lab, Northampton, MA, USA) and ggplot2 (version 3.3.2) in R 4.0.2 (https://mirrors.ustc.edu.cn/CRAN/). 1stOpt1.5 (7D - soft High Technology Inc.), a multivariate nonlinear curve fitting software was used for fitting parameters.

## 3. Results

### 3.1. Meteorological features at different elevational distributions

The meteorological data showed that the mean annual precipitation and temperature exhibited decreasing trends with increasing elevation (Fig. 1**C and 1D**). Among them, the mean annual precipitation at different elevations (low, mid, and high) were 731.92, 485.72, and 472.40 mm, respectively. The mean annual temperatures were 9.40,

**Table 2**
Average water content and the regression equation of the biomass of each component of poplar in the Mid-watershed of "One River and Two Tributaries," Tibet (Guan and Liu., 1993).

| Biomass component | Type of equation | Parameters | Water content of PB | Water content of PA |
|---|---|---|---|---|
| Stem | W = aD^b | a = 0.1798133 b = 2.251178 | 0.4635 | 0.4350 |
| Branche | W = aD^b | a = 0.0367696 b = 2.36404 | 0.5110 | 0.5050 |
| Leaf | W = aD^b | a = 0.0525442 b = 1.885001 | 0.6337 | 0.6262 |

8.97, and 7.37 ℃, respectively. The trends of meteorological elements revealed that the temperature series of the three elevation zones showed an increasing trend during the 1980–2020 period (Fig. 1**D**). Moreover, the monthly climate factors at different elevations also exhibited differences (Fig. 1**E-G**).

### 3.2. Low-frequency growth signals and their relevant indicators reveal tree growth

On the stand scale, the growth rate of tree DBH of the poplar plantations along the self-DBH gradient showed a typical unimodal pattern when $T \rightarrow g_r/m_r$ and 0, *i.e.*, with the increase in self-DBH, the growth rate first increased and then decreased (Fig. 2). The length (maximum DBH) and height (the maximum growth rate of tree DBH) of these unimodal curves were significantly different. The PB and PA plantations at low elevations both had larger maximum DBH, $m_r/g_r$ values, and mean growth rates (Table 3). Furthermore, PB may have greater adaptability, thus causing larger maximum DBH, mean growth rate of tree DBH and lifespan in different elevational distributions than PA (Table 3).

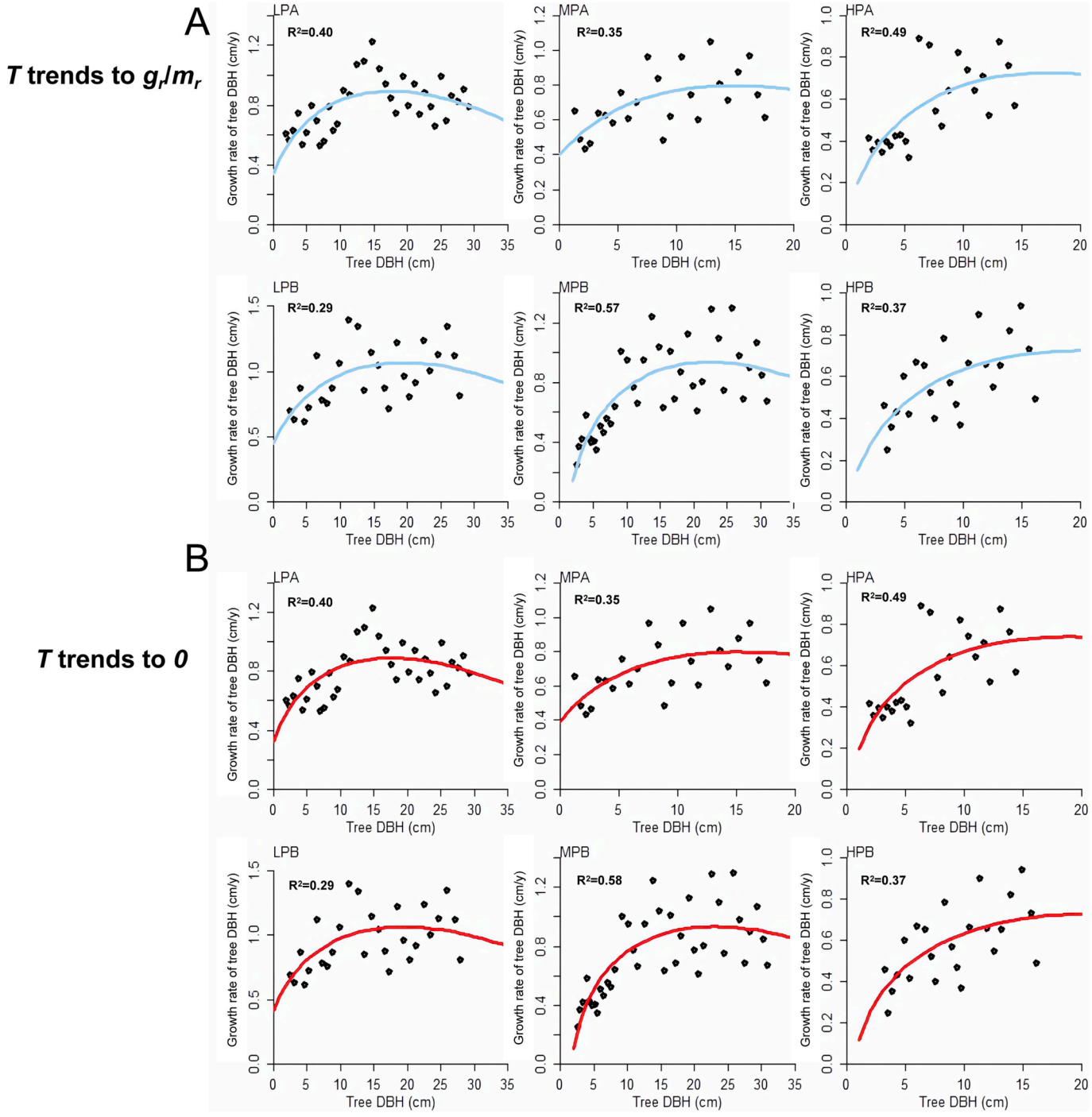


**Fig. 2.** Low-frequency growth signals of poplar plantations in different elevational distributions. (A) Low-frequency growth signals of poplar plantations in different elevational distributions when $T$ trends to $g_r/m_r$. (B) Low-frequency growth signals of poplar plantations in different elevational distributions when $T$ trends to *0*. Solid black circles are the mean growth rate of tree DBH (cm/y), and blue and red curves are low-frequency growth curves when $T \rightarrow g_r/m_r$ and 0, respectively. (For interpretation of the references to colour in this figure legend, the reader is referred to the web version of this article.)

**Table 3**
Characteristic values of unimodal curves when $T$ trends to 0 and $g_r/m_r$.

| | $T$ trends to 0 | | | | $T$ trends to $g_r/m_r$ | | | |
|---|---|---|---|---|---|---|---|---|
| Tree species | Max DBH (cm) | $m_r/g_r$ | Lifespan (years) | Mean GR (cm/y) | Max DBH (cm) | $m_r/g_r$ | Lifespan (years) | Mean GR (cm/y) |
| LPB | 70.92 | 0.27 | 51.78 | 1.37 | 68.44 | 0.15 | 94.72 | 0.72 |
| MPB | 71.56 | 0.23 | 59.60 | 1.20 | 65.51 | 0.14 | 103.17 | 0.64 |
| HPB | 67.50 | 0.19 | 72.09 | 0.94 | 61.26 | 0.11 | 124.89 | 0.49 |
| LPA | 63.82 | 0.25 | 55.78 | 1.14 | 60.94 | 0.14 | 100.72 | 0.61 |
| MPA | 59.01 | 0.24 | 57.52 | 1.03 | 54.89 | 0.14 | 101.60 | 0.54 |
| HPA | 62.87 | 0.21 | 66.16 | 0.95 | 53.49 | 0.13 | 108.78 | 0.49 |

Abbreviations: Max, maximum; GR, growth rate.

In general, compared with the classic standard chronology, the variation in high-frequency and its response to climate were similar (Fig. 3**A, 3B, and S2**), as obtained by the IGMR-U. Interestingly, for the whole Yarlung Tsangpo River basin, the radial growth of poplar plantations was more sensitive to temperature (**Fig. S2**). In addition, the low-frequency growth trends limited high-frequency signals, *i.e.*, the high-frequency variations were related to the growth rate of tree DBH (Fig. 3**C**).

Due to tree lifespan $\propto g_r/m_r$ values, two poplar plantations also followed trade-offs in tree growth rate and lifespan, *i.e.*, increased growth rates shortened tree lifespan (Table. 3). In contrast to the effect of temperature on longevity and growth rate ($P < 0.05$, Fig. 4**A and 4B**), no significant effect of precipitation was found on growth rate and longevity ($P > 0.05$, Fig. 4**C and 4D**). Therefore, temperature is a crucial factor affecting growth-lifespan trade-offs and controlling forest growth. For the whole Yarlung Tsangpo River basin, the optimal temperature of poplar plantations growth in these trade-offs was at 14.69 ℃. This result is according to the growth-lifespan trade-offs and the relationship between temperature and lifespan (Fig. 4**B and 4E**). It is where the maximum DBH could reach 75.84 cm, and the corresponding tree lifespan and mean growth rate were 62.46 years and 1.21 cm year$^{-1}$, respectively. Overall, poplar plantations may have adapted to the plateau climate by reducing growth rates and increasing longevity.

### 3.3. *Low-frequency growth signals and their relevant indicators reveal forest carbon sequestration*

With the IGM, tree ring growth was further linked to forest carbon sinks (see supplementary information). In the PB and PA plantations, a strong linear relationship could be found between the NPP data and NPP calculation when $T \rightarrow g_r/m_r$ and 0 ($P < 0.001$, adjusted $R^2 > 0.55$, Fig. 5**A and 5B**). These results adequately described the correctness of the IGMF. Moreover, **Eq. (5b)** explained the data better: when $T$ tends to $g_r/m_r$, slope values (k = 1.11) were closer to 1 than $T$ trends to 0 (k = 2.13). Therefore, in the data analyses of this study, IGMR-U was selected to characterize the iterative growth mechanism (Figs. 3, 4, 5**C, and 5D**). On the basis of these results, the current and potential maximum aboveground biomasses of poplar plantations were estimated for the Yarlung Tsangpo River basin (**Eq. (6)**). The current and potential maximum aboveground biomasses of PB plantations (6471.56 ±

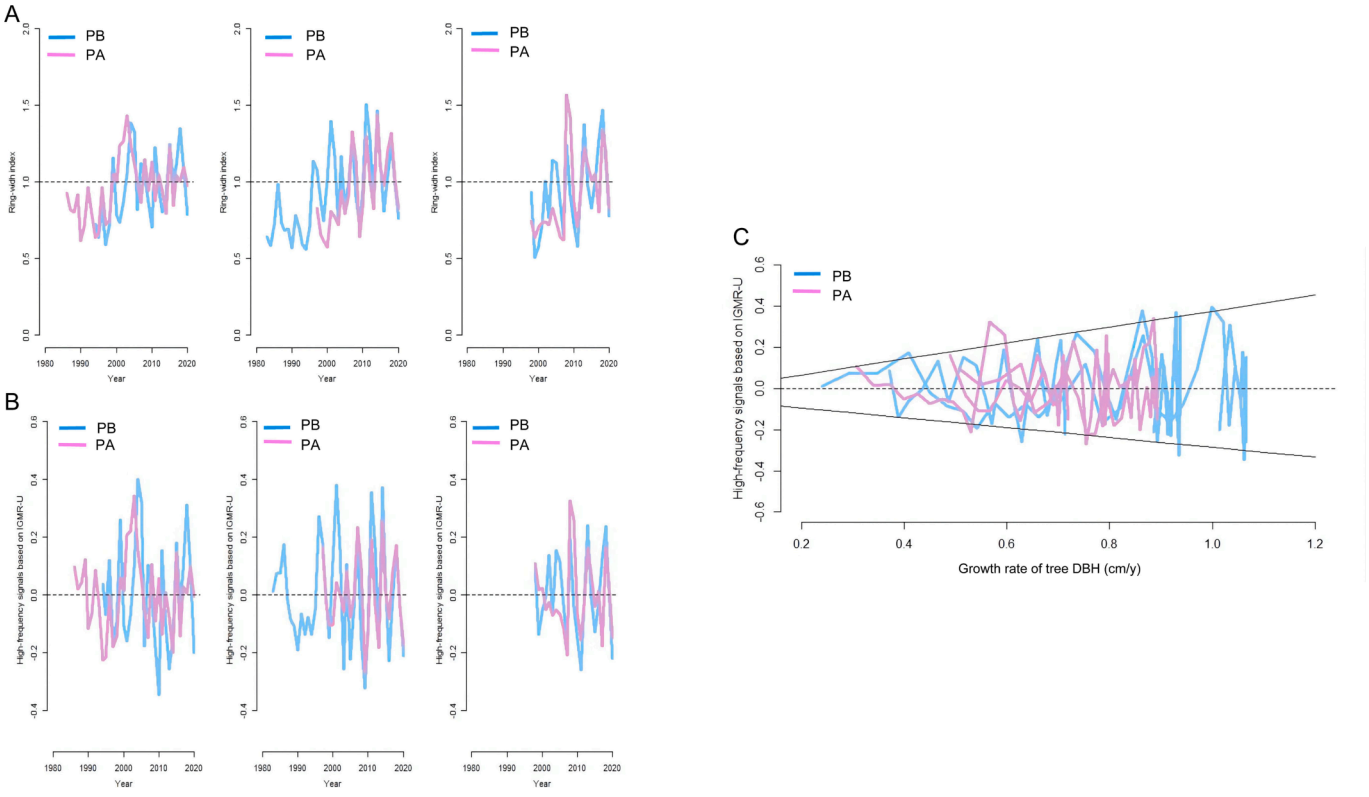


**Fig. 3.** Standard chronology, high-frequency signals based on IGMR-U, and relationship between low- and high-frequency signals. (A) Classic standard chronology. (B) High-frequency signals based on IGMR-U. (C) High-frequency signals based on IGMR-U were restricted by the height of the low-frequency growth signals. The high-frequency signals based on IGMR-U were calculated by the difference between the tree-ring growth rate and the low-frequency growth signal based on IGMR-U.

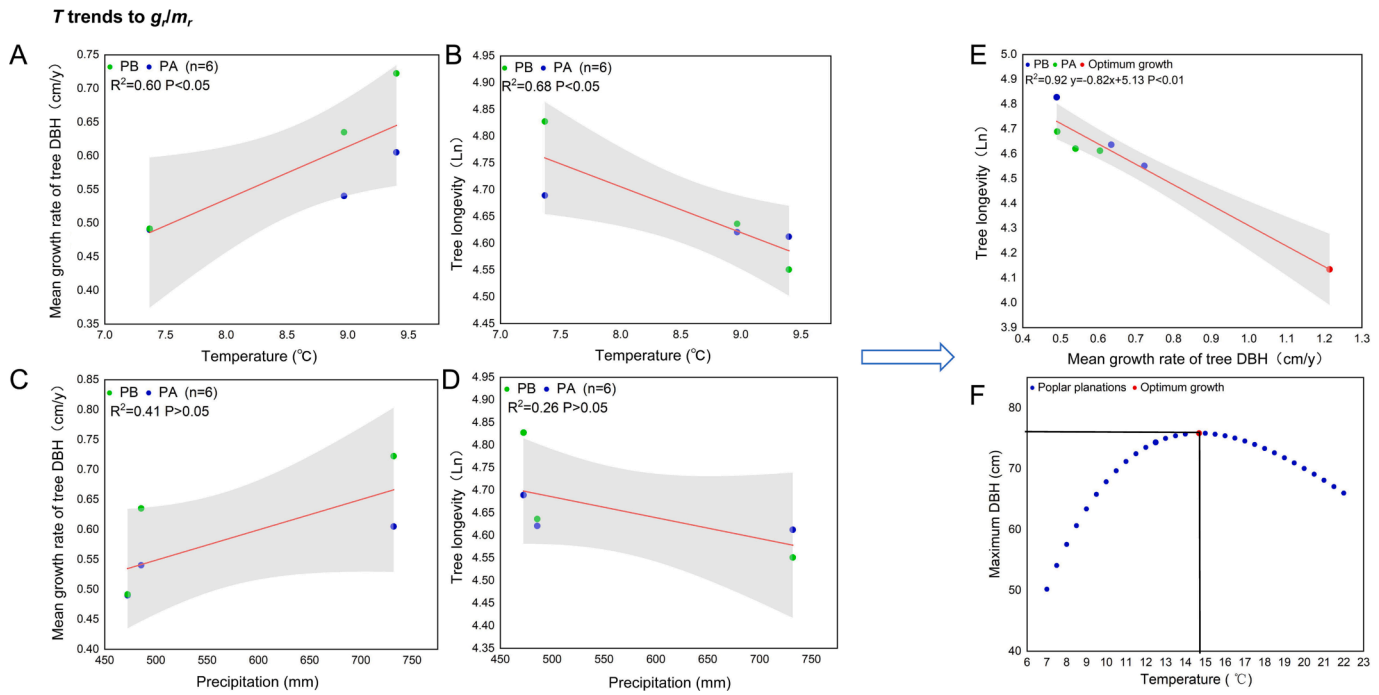


**Fig. 4.** Effects of environmental factors on growth-lifespan trade-offs and their optimal outcomes. (A) Relationship between the temperature and tree-ring growth rate. (B) Relationship between temperature and tree longevity (LN). (C) Relationship between the precipitation and tree-ring growth rate. (D) Relationship between the precipitation and tree longevity (LN). (E) Relationship between the tree-ring growth rate and tree longevity (LN). (F) The relationship between the temperature and maximum DBH. The regression line with adjusted $R^2$ is given in the figures. The shaded areas show the 95% confidence interval of the fit.

1111.97 and 11695.58 ± 1704.98 g/m$^2$, respectively) were greater than those of PA plantations (4528.68 ± 1433.83 and 9032.50 ± 2031.21 g/m$^2$, respectively), as shown in Fig. 5**C**. Furthermore, in accordance with the carbon content rate of 0.47, the current and potential maximum aboveground carbon stocks of the PB and PA plantations are shown in Fig. 5**D**. Taken together, the current aboveground carbon sequestration of plantations in Tibet based on the planting area of plantations could be estimated (3.34–4.77 Tg).

## 4. Discussion

### *4.1. Low-frequency growth signals have more profound effects on tree growth and forest carbon sequestration.*

Trees' growth trajectory (with respect to their age or size) follows a clear hump-shaped pattern. The results of this study clarified the possible kinetic mechanism behind this pattern. They highlighted the constraints of this trend on the high-frequency variations (Fig. 2 **and** Table. 2). In the models, tree size (or tree DBH) is the primary driver of growth. In fact, the size effect is closely related to resource uptake and trade-offs (Gibert et al., 2016). In some experiments, size has a greater impact on age-related declines in relative growth and net assimilation rates than cellular senescence (Mencuccini et al., 2005). The effect of environmental factors on the growth rate inevitably feeds back to size (Shu et al., 2019). Thus, the size-growth curve should change overall with the climate and have more profound effects on tree growth and forest carbon sequestration. Meanwhile, tree longevity and/or DBH determine the height and length of the unimodal growth curve.

When trees' age or size increase, the annual ring width decrease as the wood is allocated around an ever-increasing circumference (Wang et al. 2017). This effect of age (or size) on tree growth is usually considered to be climate-independent (Peters et al., 2015). To highlight the influence of climate on growth, many studies typically remove age effects through various detrending methods (Fang et al., 2018; Tao et al., 2022; Wang et al., 2017). However, our results suggest that variation in tree radial growth with age/size is not climate independent. The best climate at low elevations increased the length and height of the unimodal growth curve. Poplar plantations at low elevations both had the largest maximum DBH and mean growth rates (Fig. 2 **and** Table 2). These findings revealed that the size-growth curve should change overall with the climate and implied a major control of growth by tree size. Moreover, the high-frequency variations were related to the height of the unimodal growth curve, indicating that changes in low-frequency growth may affect the environmental sensitivity of height-frequency signals (Fig. 3**C**). Therefore, low-frequency growth signals have more profound effects on tree growth.

Low-frequency growth signals also have more profound effects on forest carbon sequestration. In this study, tree ring growth was successfully linked to forest carbon sequestration ($P < 0.001$, adjusted $R^2 > 0.55$, Fig. 5**A and 5B**), which not only verified the correctness of the IGM for forest NPP but also indicated that forest NPP is strongly correlated with the low-frequency signal. For a theoretical explanation, their expression levels with respect to time conformed to the Richards and Gompertz equations (supplementary information), where tree age, temperature (strongly correlated with growing season length) (Michaletz et al., 2017), and *r* are the three basic axes that explain the variation in *f(r)*.

### *4.2. Low-temperature limits tree growth and forest carbon sequestration*

In general, the future evolution of forest carbon sequestration depends critically on the tree growth rate and lifespan response to the future climate (Brienen et al., 2020; Locosselli et al., 2020; Lorimer et al., 2001). Placing the results into the global context of growth-lifespan trade-offs, the poplar plantations on the Tibetan Plateau were observed to be closer to the global results' lower boundary (Locosselli et al., 2020). As broadleaf tree species, poplars grow faster and live shorter than conifers. However, in the alpine ecosystem, the trade-off strategy of poplars moves closer to conifers, suggesting that poplars have strong ecological adaptability. Temperature and precipitation are

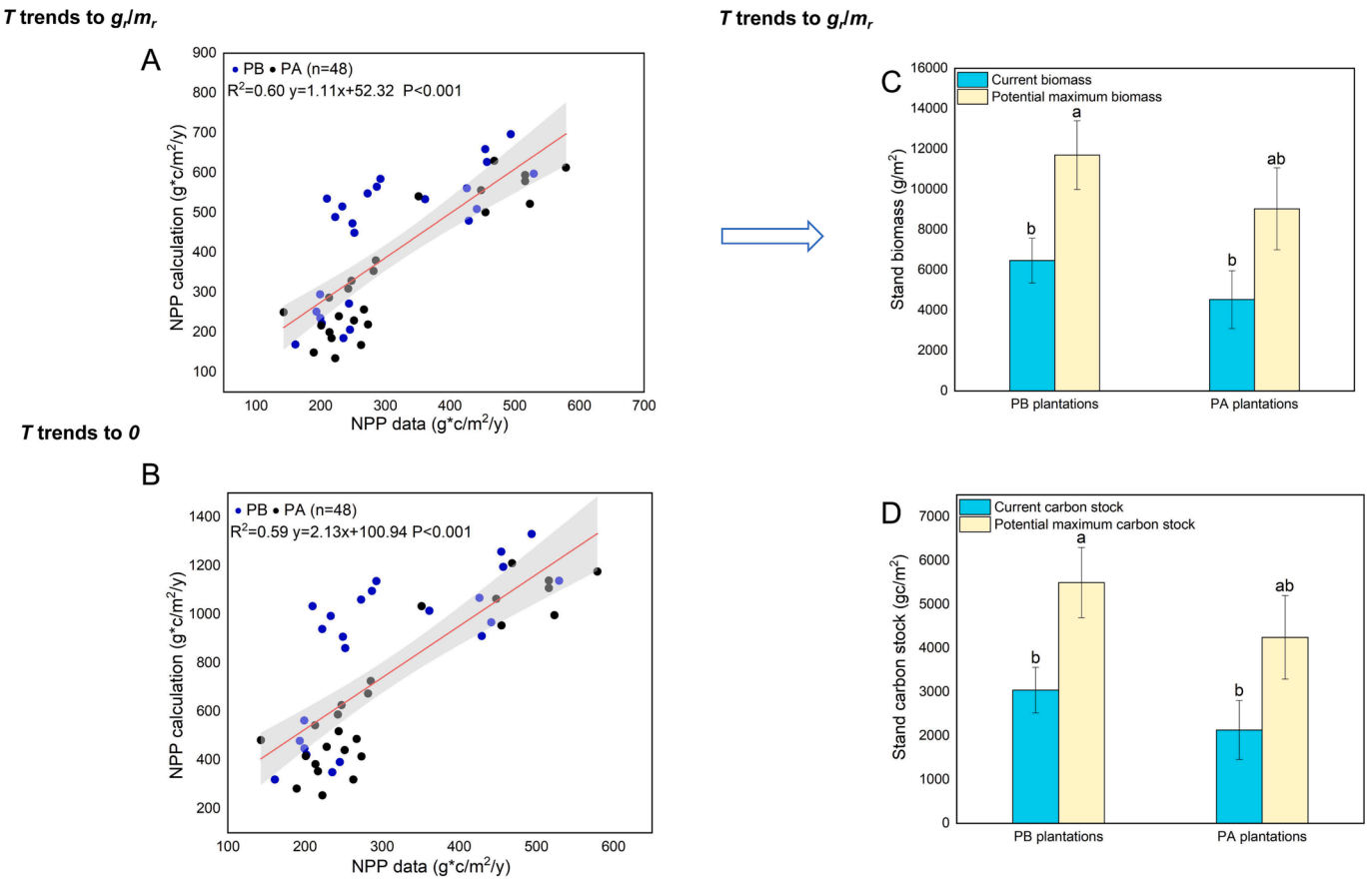


**Fig. 5.** Verification and application of IGM for forest NPP. (A) The relationship between the NPP calculation and NPP data of PB and PA plantations when *T* trends to $g_r/m_r$. (B) Relationship between the NPP calculation and NPP data of PB and PA plantations when *T* trends to 0. The regression line with adjusted $R^2$ is given in the figures. The shaded areas show the 95% confidence interval of the fit. (C) The current and potential maximum aboveground biomass of poplar plantations. (D) The current and potential maximum aboveground carbon stock of poplar plantations. Values are the mean ± SE. Different lowercase letters indicate significant differences ($P < 0.05$). The Kruskal-Wallis test was used.

the main climatic factors that affect tree growth processes. However, in this study area, no correlations were found between mean growth rate and longevity with precipitation ($P > 0.05$, Fig. 4**C and 4D**). This may be because the poplar plantations are mainly planted on relatively wet riverbanks, which causes insensitivity to precipitation variability. Temperature, however, substantially impacts tree growth and longevity ($P < 0.05$, Fig. 4**A and 4B**). Similar to previous studies, it is not surprising that temperature is a dominant constraint on plant growth and productivity at high elevation and latitude (Huang et al., 2019; Liang et al., 2008; Li et al., 2012; Shi et al., 2015). Higher temperatures, particularly in plateau regions, could facilitate snow melting and subsequent plant photosynthesis, cell division, and the accumulation of trunk materials, resulting in larger radial growth (Korner, 1998; Kroner and Way, 2016; Ponocna et al., 2016; Shrestha et al., 2015; Yu et al., 2013, Zhang et al., 2015). In this study, the meteorological data showed that the mean annual temperature exhibited decreasing trends with increasing elevation. Therefore, under the long-term effects of environmental factors, the length and height of unimodal growth curves at low elevations were the largest, and the forest carbon sequestration also showed decreasing trends with increasing elevation (Fig. S3**A**). Due to the control function of temperature on lifespan and the inherent trade-offs of growth-lifespan, the best value for tree growth was 14.69 ℃ (Fig. 4**F**). Similar to numerous other studies, temperature plays an essential role in trade-offs (Brienen et al., 2020; Di Filippo et al., 2015; Locosselli et al., 2020). For physiological explanations, under low-temperature stress, plant growth could be restricted by carbon source or/sink limitations (Fig. 6) (Green and Keenan, 2022). On the one hand, the lower temperature could limit photosynthesis, which decreases carbon source for plant growth (*i.e.*, carbon source limitation). On the other hand, trees tend to reduce growth rates but use energy and nutrients to increase carbon storage (*i.e.*, carbon sink limitation). Theoretically, longevity terms contain the parameter $m_r$, which is positively correlated with temperature (Fig. 6). However, increasing temperatures may increase tree mortality rates. For instance, under high temperatures, trees may reduce growth and compensate for increasing water losses by increasing VPD and forcing stomata to close, which could result in decreased carbon assimilation rates and may kill trees due to carbon starvation (Allen et al., 2015; McDowell et al., 2008). Therefore, as climate warming proceeds, a moderate temperature rise could be expected to benefit poplar plantation growth on the Tibetan Plateau.

### *4.3. Implications for the reasonable plantation and management of poplar plantations on the Tibetan Plateau*

The premise of successful afforestation efforts is understanding tree species' suitability to the local environments and their ecological responses. As they are adaptative, fast-growing, and easy to survive, the difference in growth is an important basis for evaluating the quality of afforestation. Theoretical indicators based on IGM and tree radial growth could be used to evaluate the growth quality of different plantation species. Moreover, the potential forest biomass could be predicted after combining the stand density based on these indicators. Collectively, our results showed that under similar habits, the maximum DBH, mean growth rate, and biomass of the PB plantation were greater (Table 3**,** Fig. 5**C and 5D**). This indicated that PB might be more sensitive to plateau climate, thus having a stronger resource acquisition and

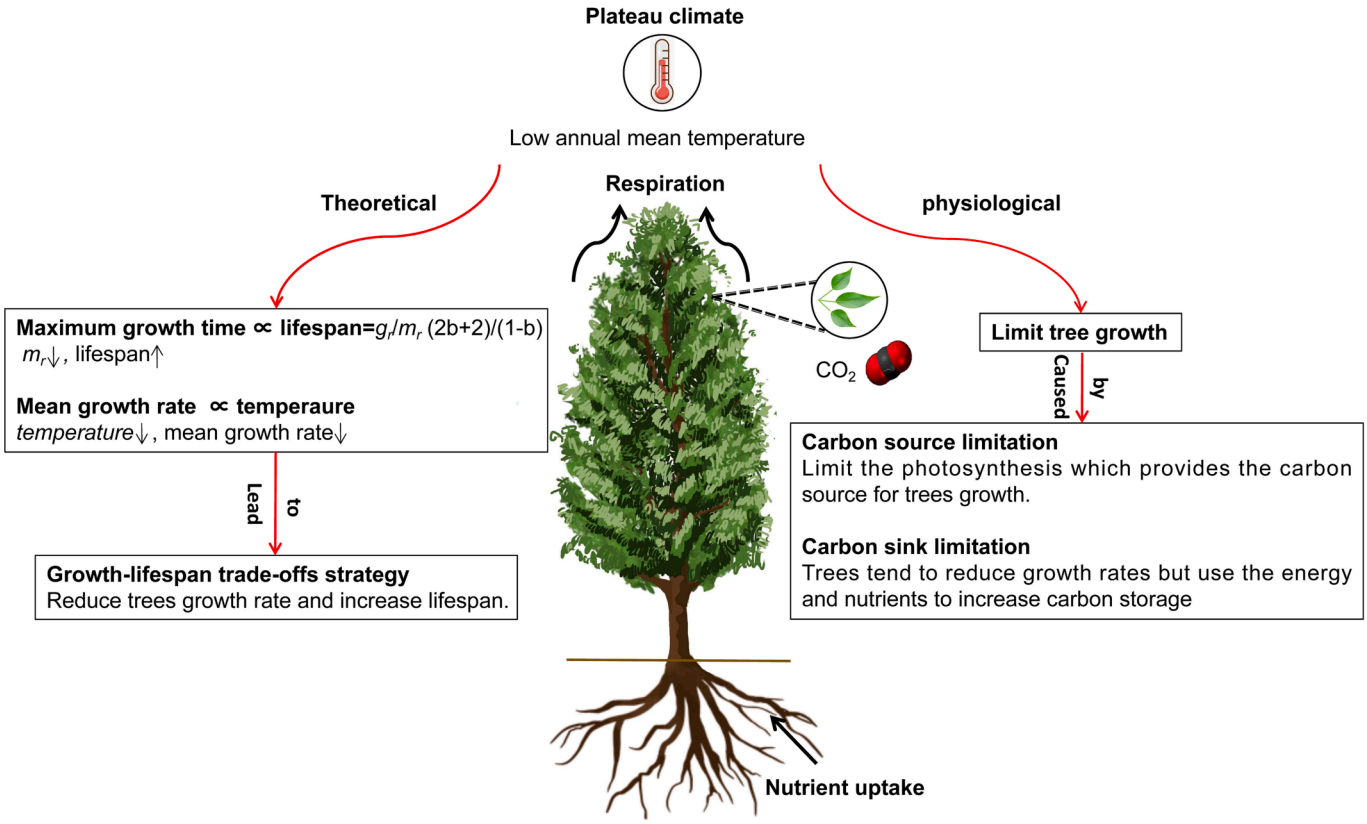


**Fig. 6.** Schematic diagram of the iterative growth mechanism and possible physiological responses of poplar in a plateau climate. The left side shows the responses of the iterative growth mechanism under the plateau climate. The right side shows possible physiological responses under the plateau climate.

adjusted ability and distributing more energy and nutrients for their growth than PA in plateau climate. The main reason for this may be related to heterosis. PB was bred by cross-breeding *P. nigra* var. *italica* (Moench) Koehne and *P. cathayana* Rehd, which have the advantages of fast growth, high adaptation, and disease resistance, making it more suitable for afforestation efforts in alpine regions (Liu et al., 2022). Therefore, for successful afforestation efforts in sensitive high-elevation areas, it is necessary to "adaptation to local conditions." PB species should be considered in future afforestation on the Tibetan Plateau. In addition, the effective management of poplar plantations will help to maintain the stability of plantations, as well as the high-quality development of the Tibetan Plateau. Recent studies have shown that planting density not only affects tree growth but also affects the response of trees to various stresses (Feng et al., 2016; Navarro-Cerrillo et al., 2020; Li et al., 2021). If afforestation managers could plan properly and control planting density, forest degradation could be improved effectively (Che et al., 2022; Navarro-Cerrillo et al., 2020). In this study, forest potential maximum biomass showed a declined trend with increasing planting density ($P < 0.05$, Fig. S3**B**). Consequently, to prevent plantation degradation, appropriate thinning should be considered.

### *4.4. IGM and its extension for assessing forest carbon dynamics*

Using the IGM, tree-ring dynamics were linked to forest NPP to obtain some crucial details of tree growth and forest carbon sequestration (**Eq.** (6)). These details, such as lifespan, growth rate, and respiration, are important derivatives of the forest's current carbon sink assessment. Although the acquisition of forest NPP by remote sensing monitoring is a common method, it cannot directly reflect the internal mechanism of tree growth and emphasizes the profound effects of low-frequency growth signals on tree growth and forest carbon sequestration. Therefore, combining remote sensing with IGM to assess and calibrate forest NPP is proposed. Moreover, previous studies on plantations on the Tibetan Plateau have mainly focused on the soil (He et al., 2021; Liu et al., 2022; Xu et al., 2010), with little research on the growth trends of plantations. Overall, IGM-based tree and forest growth models should be very useful for assessing the tree growth and forest carbon sequestration of plantations that lack effective monitoring. However, this study still has potential limitations. Many core samples with unclear demarcated annual rings were abandoned because poplar is a diffuse-porous species. This decision could inevitably reduce the precision of the results. Overall, a large sample size, clear tree-ring width, and longer time scales would reduce the fitting error and make the model-based indicators more accurate. In addition, the physiological and biochemical details behind model parameters still need to be clarified. These further studies have great implications for understanding and predicting the global forest carbon budget in the context of global climate change.

## 5. Conclusions

In this study, low-frequency growth signals and their profound effects on tree growth and forest carbon sequestration of poplar plantations in the Yarlung Tsangpo River basin were revealed based on tree-ring dynamics, IGM and its extension, and NPP data. (i) The low-frequency growth signals of poplar plantations all followed a single-mode pattern over the DBH gradient. The length and height of unimodal growth curves varied overall with the environment. These signals could affect the climate sensitivity of high-frequency signals. (ii) Poplars have adapted to the plateau climate by reducing their growth rates and increasing longevity. Temperature is the key factor affecting the trade-offs, and the best temperature for growth is 14.69 ℃. (iii) PB was a more suitable poplar species on the Tibetan Plateau. The selection of PB species should be mainly considered in future afforestation efforts on the Tibetan Plateau. Moreover, appropriate thinning should also be

considered to prevent plantation degradation. In summary, tree-ring low-frequency signals should not be ignored in future studies, and their relevant indicators have great implications for understanding and predicting the global forest carbon budget in the context of global climate change. The results of this study provide a certain basis for reasonable plantations in sensitive high-elevation areas. It also has important theoretical and practical significance for properly assessing the ecological contribution of afforestation activities on the Tibetan Plateau.

## Funding

This work was supported by the Second Tibetan Plateau Scientific Expedition and Research Program (2019QZKK0404), the Strategic Priority Research Program of the Chinese Academy of Sciences (XDA20020401), Science and Technology Major Project of Tibetan Autonomous Region of China (XZ202201ZD0005G02) and the Fundamental Research Funds for the Central Universities.

## CRediT authorship contribution statement

**Yuan Yao:** Performed the experiments, Collected and analyzed the data, Wrote the original manuscript. **Shumiao Shu:** Conceptualization, Methodology, Data curation, Software, Validation, Writing – review & editing. **Wenzhi Wang:** Software, Data curation, Writing – review & editing. **Ruixuan Liu:** Performed some laboratory work, Data curation. **Yuelin Wang:** Analyzed the data. **Xiaodan Wang:** Funding acquisition, Manuscript revised. **Sheng Zhang:** Designed the experiment, Funding acquisition, Revised manuscript.

## Declaration of Competing Interest

The authors declare that they have no known competing financial interests or personal relationships that could have appeared to influence the work reported in this paper.

## Data availability

Data will be made available on request.

## Appendix A. Supplementary data

Supplementary data to this article can be found online at https://doi.org/10.1016/j.ecolind.2023.109930.

## References

Allen, C.D., Breshears, D.D., McDowell, N.G., 2015. On underestimation of global vulnerability to tree mortality and forest die-off from hotter drought in the Anthropocene. Ecosphere 6, 129. https://doi.org/10.1890/ES15-00203.1.

Amthor, J.S., 2000. The Mccree-de Wit-Penning de Vries-Thornley respiration paradigms: 30 years later. Ann Bot-London 86, 1–20. https://doi.org/10.1006/anbo.2000.1175.

Brienen, R.J.W., Caldwell, L., Duchesne, L., Voelker, S., Barichivich, J., Baliva, M., Ceccantini, G., Di Filippo, A., Helama, S., Locosselli, G.M., Lopez, L., Piovesan, G., Schöngart, J., Villalba, R., Gloor, E., 2020. Forest carbon sink neutralized by pervasive growth-lifespan trade-offs. Nat. Commun. 11 (1) https://doi.org/10.1038/s41467-020-17966-z.

Cabon, A., Kannenberg, S.A., Arain, A., Babst, F., Baldocchi, D., Belmecheri, S., Delpierre, N., Guerrieri, R., Maxwell, J.T., McKenzie, S., Meinzer, F.C., Moore, D.J. P., Pappas, C., Rocha, A.V., Szejner, P., Ueyama, M., Ulrich, D., Vincke, C., Voelker, S.L., Wei, J.S., Woodruff, D., Anderegg, W.R.L., 2022. Cross-biome synthesis of source versus sink limits to tree growth. Science 376, 758–761. https://doi.org/10.1126/science.abm4875.

Camarero, J.J., Gazol, A., Linares, J.C., Fajardo, A., Colangelo, M., Valeriano, C., Sanchez-Salguero, R., Sanguesa-Barreda, G., Granda, E., Gimeno, T.E., 2021. Differences in temperature sensitivity and drought recovery between natural stands and plantations of conifers are species-specific. Sci. Total Environ. 796, 148930 https://doi.org/10.1016/j.scitotenv.2021.148930.

Cannell, M.G.R., Thornley, J.H.M., 2000. Modelling the components of plant respiration: Some guiding principles. Ann Bot-London 85, 45–54. https://doi.org/10.1006/anbo.1999.0996.

Che, C.W., Xiao, S.C., Ding, A.J., Peng, X.M., Su, J.R., 2022. The characteristics of radial growth and ecological response of *Caragana korshinskii* Kom. Under different precipitation gradient in the western Loess Plateau, China. Front. Plant Sci. 13, 862529 https://doi.org/10.3389/fpls.2022.862529.

Clarke, A., 2019. Energy flow in growth and production. Trends Ecol. Evol. 34, 502–509. https://doi.org/10.1016/j.tree.2019.02.003.

Debeljak, M., Poljanec, A., Zenko, B., 2014. Modelling forest growing stock from inventory data: a data mining approach. Ecol. Indic. 41, 30–39. https://doi.org/10.1016/j.ecolind.2014.01.010.

Di Filippo, A., Pederson, N., Baliva, M., Brunetti, M., Dinella, A., Kitamura, K., Knapp, H. D., Schirone, B., Piovesan, G., 2015. The longevity of broadleaf deciduous trees in Northern Hemisphere temperate forests: Insights from tree-ring series. Front. Ecol. Evol. 3, 46. https://doi.org/10.3389/fevo.2015.00046.

Fang, O.Y., Alfaro, R.I., Zhang, Q.B., 2018. Tree rings reveal a major episode of forest mortality in the late 18th century on the Tibetan Plateau. Global Planet. Change 163, 44–50. https://doi.org/10.1016/j.gloplacha.2018.02.004.

Feng, X.M., Fu, B.J., Piao, S.L., Wang, S.H., Ciais, P., Zeng, Z.Z., Lu, Y.H., Zeng, Y., Li, Y., Jiang, X.H., Wu, B.F., 2016. Revegetation in China's Loess Plateau is approaching sustainable water resource limits. Nat. Clim. Chang. 6, 1019–1022. https://doi.org/10.1038/nclimate3092.

Gibert, A., Gray, E.F., Westoby, M., Wright, I.J., Falster, D.S., 2016. On the link between functional traits and growth rate: meta-analysis shows effects change with plant size, as predicted. J. Ecol. 104, 1488–1503. https://doi.org/10.1111/1365-2745.12594.

Gower, S.T., Vogel, J.G., Norman, J.M., Kucharik, C.J., Steele, S.J., Stow, T.K., 1997. Carbon distribution and aboveground net primary production in aspen, jack pine, and black spruce stands in Saskatchewan and Manitoba, Canada. J. Geophys. Res.-Atmos. 102, 29029–29041. https://doi.org/10.1029/97JD02317.

Green, J.K., Keenan, T.F., 2022. The limits of forest carbon sequestration. Science 376, 692–693. https://doi.org/10.1126/science.abo6547.

Guan, H.S., Liu, Y.L., 1993. Biomass of poplar plantations in the "One River and Two Tributaries". Tibet. For Sci Technol (In Chinese) 09, 20–22. https://doi.org/10.13456/j.cnki.lykt.1993.09.009.

Hajima, T., Tachiiri, K., Ito, A., Kawamiya, M., 2014. Uncertainty of concentration-terrestrial carbon feedback in earth system models. J. Clim. 27, 3425–3445. https://doi.org/10.1175/JCLI-D-13-00177.1.

He, Y.J., Han, X.R., Wang, X.P., Wang, L.Q., Liang, T., 2021. Long-term ecological effects of two artificial forests on soil properties and quality in the eastern Qinghai-Tibet Plateau. Sci. Total Environ. 796, 148986 https://doi.org/10.1016/j.scitotenv.2021.148986.

Herault, B., Bachelot, B., Poorter, L., Rossi, V., Bongers, F., Chave, J., Paine, C.E.T., Wagner, F., Baraloto, C., 2011. Functional traits shape ontogenetic growth trajectories of rain forest tree species. J. Ecol. 99, 1431–1440. https://doi.org/10.1111/j.1365-2745.2011.01883.x.

Holmes, R.L., 1983. Computer-assisted quality control in tree-ring dating and measurement. Tree-Ring Bull. 43, 69–78.

Huang, M.T., Piao, S.L., Ciais, P., Penuelas, J., Wang, X.H., Keenan, T.F., Peng, S.S., Berry, J.A., Wang, K., Mao, J.F., Alkama, R., Cescatti, A., Cuntz, M., De Deurwaerder, H., Gao, M.D., He, Y., Liu, Y.W., Luo, Y.Q., Myneni, R.B., Niu, S.L., Shi, X.Y., Yuan, W.P., Verbeeck, H., Wang, T., Wu, J., Janssens, I.A., 2019. Air temperature optima of vegetation productivity across global biomes. Nat. Ecol. Evol. 3, 772–779. https://doi.org/10.1038/s41559-019-0838-x.

Ipcc, 2006. 2006 IPCC Guidelines for National Greenhouse Gas Inventories. Prepared by the National Greenhouse Gas Inventories Programme, IGES, Japan.

Johnson, D.J., Needham, J., Xu, C.G., Massoud, E.C., Davies, S.J., Anderson-Teixeira, K. J., Bunyavejchewin, S., Chambers, J.Q., Chang-Yang, C.H., Chiang, J.M., Chuyong, G.B., Condit, R., Cordell, S., Fletcher, C., Giardina, C.P., Giambelluca, T. W., Gunatilleke, N., Gunatilleke, S., Hsieh, C.F., Hubbell, S., Inman-Narahari, F., Kassim, A.R., Katabuchi, M., Kenfack, D., Litton, C.M., Lum, S., Mohamad, M., Nasardin, M., Ong, P.S., Ostertag, R., Sack, L., Swenson, N.G., Sun, I.F., Tan, S., Thomas, D.W., Thompson, J., Umana, M.N., Uriarte, M., Valencia, R., Yap, S., Zimmerman, J., McDowell, N.G., McMahon, S.M., 2018. Climate sensitive size-dependent survival in tropical trees. Nat. Ecol. Evol. 2, 1436–1442. https://doi.org/10.1038/s41559-018-0626-z.

Korner, C., 1998. A re-assessment of high elevation treeline positions and their explanation. Oecologia 115, 445–459. https://doi.org/10.1007/s004420050540.

Kroner, Y., Way, D.A., 2016. Carbon fluxes acclimate more strongly to elevated growth temperatures than to elevated $CO_2$ concentrations in a northern conifer. Glob. Chang. Biol. 20, 2913–2928. https://doi.org/10.1111/gcb.13215.

Li, C.J., Fu, B.J., Wang, S., Stringer, L.C., Wang, Y.P., Li, Z.D., Liu, Y.X., Zhou, W.X., 2021. Drivers and impacts of changes in China's drylands. Nat Rev Earth Env 2, 858–873. https://doi.org/10.1038/s43017-021-00226-z.

Li, F.P., Xu, Z.X., Feng, Y.C., Liu, M., Liu, W.F., 2013. Changes of land cover in the Yarlung Tsangpo River basin from 1985 to 2005. Environ. Earth Sci. 68, 181–188. https://doi.org/10.1007/s12665-012-1730-z.

Li, Z.S., Zhang, Q.B., Ma, K., 2012. Tree-ring reconstruction of summer temperature for AD 1475–2003 in the central Hengduan Mountains, Northwestern Yunnan, China. Clim. Change 110, 455–467. https://doi.org/10.1007/s10584-011-0111-z.

Liang, S.L., Cheng, J., Jia, K., Jiang, B., Liu, Q., Xiao, Z.Q., Yao, Y.J., Yuan, W.P., Zhang, X.T., Zhao, X., Zhou, J., 2021. The Global Land and Surface Satellite (GLASS) products suite. B Am Meteorol Soc 102, E323–E337. https://doi.org/10.1175/BAMS-D-18-0341.

Liang, E.Y., Shao, X.M., Qin, N.S., 2008. Tree-ring based summer temperature reconstruction for the source region of the Yangtze River on the Tibetan Plateau. Global Planet. Change 61, 313–320. https://doi.org/10.1016/j.gloplacha.2007.10.008.

Liao, J., Cai, Z.Y., Song, H.F., Zhang, S., 2020. Poplar males and willow females exhibit superior adaptation to nocturnal warming than the opposite sex. Sci. Total Environ. 717, 137179 https://doi.org/10.1016/j.scitotenv.2020.137179.

Ling, H.B., Zhang, P., Guo, B., Xu, H.L., Ye, M., Deng, X.Y., 2017. Negative feedback adjustment challenges reconstruction study from tree rings: A study case of response of *Populus euphratica* to river discontinuous flow and ecological water conveyance. Sci. Total Environ. 574, 109–119. https://doi.org/10.1016/j.scitotenv.2016.09.043.

Liu, Y., Wang, Y.S., Wei, L.S., Shen, T., Shu, Q.F., Huang, A.B., Jia, Y., 2020. River capture in the middle reaches of the palaeo-Yarlung Zangbo River. Roy Soc Open Sci 7, 191753. https://doi.org/10.1098/rsos.191753.

Liu, J.T., Xu, Z.X., Bai, J.R., Peng, D.Z., Ren, M.F., 2018. Assessment and correction of the PERSIANN-CDR product in the Yarlung Zangbo River basin. China. Remote Sens-Basel 10, 2031. https://doi.org/10.3390/rs10122031.

Liu, R.X., Yao, Y., Li, Q., Cai, Z.Y., We, D., Wang, X.D., Zhang, S., 2022. Rhizosphere soil microbes benefit carbon and nitrogen sinks under long-term afforestation on the Tibetan Plateau. Catena 220, 106705. https://doi.org/10.1016/j.catena.2022.106705.

Locosselli, G.M., Brienen, R.J.W., Leite, M.D., Gloor, M., Krottenthaler, S., de Oliveira, A. A., Barichivich, J., Anhuf, D., Ceccantini, G., Schongart, J., Buckeridge, M., 2020. Global tree-ring analysis reveals rapid decrease in tropical tree longevity with temperature. P Natl Acad Sci USA 117, 33358–33364. https://doi.org/10.1073/pnas.2003873117.

Lorimer, C.G., Dahir, S.E., Nordheim, E.V., 2001. Tree mortality rates and longevity in mature and old-growth hemlock–hardwood forests. J. Ecol. 89, 960–971. https://doi.org/10.1046/j.0022-0477.2001.00619.x.

Lu, M., Zhou, X.H., Yang, Q., Li, H., Luo, Y.Q., Fang, C.M., Chen, J.K., Yang, X., Li, B., 2013. Responses of ecosystem carbon cycle to experimental warming: a meta-analysis. Ecology 94, 726–738. https://doi.org/10.1890/12-0279.1.

Ma, X.P., Asano, M., Tamura, K., Zhao, R.N., Nakatsuka, H., Wuyunna.,, Wang, T., 2020. Physicochemical properties and micromorphology of degraded alpine meadow soils in the Eastern Qinghai-Tibet Plateau. Catena 194. https://doi.org/10.1016/j.catena.2020.104649.

Matsushita, M., Takata, K., Hitsuma, G., Yagihashi, T., Noguchi, M., Shibata, M., Masaki, T., 2015. A novel growth model evaluating age-size effect on long-term trends in tree growth. Funct. Ecol. 29, 1250–1259. https://doi.org/10.1111/1365-2435.12416.

McDowell, N., Pockman, W.T., Allen, C.D., Breshears, D.D., Cobb, N., Kolb, T., Plaut, J., Sperry, J., West, A., Williams, D.G., Yepez, E.A., 2008. Mechanisms of plant survival and mortality during drought: why do some plants survive while others succumb to drought? New Phytol. 178, 719–739. https://doi.org/10.1111/j.1469-8137.2008.02436.x.

Mencuccini, M., Martinez-Vilalta, J., Vanderklein, D., Hamid, H.A., Korakaki, E., Lee, S., Michiels, B., 2005. Size-mediated ageing reduces vigour in trees. Ecol. Lett. 8, 1183–1190. https://doi.org/10.1111/j.1461-0248.2005.00819.x.

Michaletz, S.T., Cheng, D.L., Kerkhoff, A.J., Enquist, B.J., 2014. Convergence of terrestrial plant production across global climate gradients. Nature 512, 39–43. https://doi.org/10.1038/nature13470.

Michaletz, S.T., Kerkhoff, A.J., Enquist, B.J., 2017. Drivers of terrestrial plant production across broad geographical gradients. Glob. Ecol. Biogeogr. 27, 166–174. https://doi.org/10.1111/geb.12685.

Mori, S., Yamaji, K., Ishida, A., Prokushkin, S.G., Masyagina, O.V., Hagihara, A., Hoque, A.T.M.R., Suwa, R., Osawa, A., Nishizono, T., Ueda, T., Kinjo, M., Miyagi, T., Kajimoto, T., Koike, T., Matsuura, Y., Toma, T., Zyryanova, O.A., Abaimov, A.P., Awaya, Y., Araki, M.G., Kawasaki, T., Chiba, Y., Umari, M., 2010. Mixed-Power Scaling of whole-plant respiration from seedlings to giant trees. P Natl Acad Sci USA 107, 1447–1451. https://doi.org/10.1073/pnas.0902554107.

Navarro-Cerrillo, R.M., Manzanedo, R.D., Rodriguez-Vallejo, C., Gazol, A., Palacios-Rodriguez, G., Camarero, J.J., 2020. Competition modulates the response of growth to climate in pure and mixed *Abies pinsapo* subsp. maroccana forests in northern Morocco. Forest Ecol Manag 459, 117847. https://doi.org/10.1016/j.foreco.2019.117847.

Overpeck, J.T., 2013. Climate science: the challenge of hot drought. Nature 503, 350–351. https://doi.org/10.1038/503350a.

Peltier, D.M.P., Ogle, K., 2020. Tree growth sensitivity to climate is temporally variable. Ecol. Lett. 23, 1561–1572. https://doi.org/10.1111/ele.13575.

Peters, R.L., Groenendijk, P., Vlam, M., Zuidema, P.A., 2015. Detecting long-term growth trends using tree rings: a critical evaluation of methods. Glob. Chang. Biol. 21, 2040–2054. https://doi.org/10.1111/gcb.12826.

Piao, S.L., Luyssaert, S., Ciais, P., Janssens, I.A., Chen, A.P., Cao, C., Fang, J.Y., Friedlingstein, P., Luo, Y.Q., Wang, S.P., 2010. Forest annual carbon cost: a global-scale analysis of autotrophic respiration. Ecology 91, 652–661. https://doi.org/10.1890/08-2176.1.

Ponocna, T., Spyt, B., Kaczka, R., Buntgen, U., Treml, V., 2016. Growth trends and climate responses of Norway spruce along elevational gradients in East-Central Europe. Trees-Struct Funct 30, 1633–1646. https://doi.org/10.1007/s00468-016-1396-3.

Richardson, A.D., Hufkens, K., Milliman, T., Aubrecht, D.M., Furze, M.E., Seyednasrollah, B., Krassovski, M.B., Latimer, J.M., Nettles, W.R., Heiderman, R.R., Warren, J.M., Hanson, P.J., 2018. Ecosystem warming extends vegetation activity but heightens vulnerability to cold temperatures. Nature 560, 368–371. https://doi.org/10.1038/s41586-018-0399-1.

Santini, F., Shestakova, T.A., Dashevskaya, S., Notivol, E., Voltas, J., 2020. Dendroecological and genetic insights for future management of an old-planted forest of the endangered Mediterranean fir *Abies pinsapo*. Dendrochronologia 63, 125754. https://doi.org/10.1016/j.dendro.2020.125754.

Shi, C.M., Masson-Delmotte, V., Daux, V., Li, Z.S., Carre, M., Moore, J.C., 2015. Unprecedented recent warming rate and temperature variability over the east Tibetan Plateau inferred from Alpine treeline dendrochronology. Clim Dynam 45, 1367–1380. https://doi.org/10.1007/s00382-014-2386-z.

Shi, P.J., Men, X.Y., Sandhu, H.S., Chakraborty, A., Li, B.L., Fang, O.Y., Sun, Y.C., Ge, F., 2013. The "general" ontogenetic growth model is inapplicable to crop growth. Ecol. Model. 266, 1–9. https://doi.org/10.1016/j.ecolmodel.2013.06.025.

Shrestha, K.B., Hofgaard, A., Vandvik, V., 2015. Tree-growth response to climatic variability in two climatically contrasting treeline ecotone areas, central Himalaya. Nepal. Can J Forest Res 45, 1643–1653. https://doi.org/10.1139/cjfr-2015-0089.

Shu, S.M., Zhu, W.Z., Wang, W.Z., Jia, M., Zhang, Y.Y., Sheng, Z.L., 2019. Effects of tree size heterogeneity on carbon sink in old forests. Forest Ecol Manag 432, 637–648. https://doi.org/10.1016/j.foreco.2018.09.023.

Shu, S.M., Zhu, W.Z., Kontsevich, G., Zhao, Y.Y., Wang, W.Z., Zhao, X.X., Wang, X.D., 2021. A discrete model of ontogenetic growth. Ecol. Model. 460, 109752 https://doi.org/10.1016/j.ecolmodel.2021.109752.

Sobel, A.H., Camargo, S.J., Hall, T.M., Lee, C.Y., Tippett, M.K., Wing, A.A., 2016. Human influence on tropical cyclone intensity. Science 353, 242–246. https://doi.org/10.1126/science.aaf6574.

Tao, W.J., Mao, K.S., He, J., Smith, N.G., Qiao, Y.X., Guo, J., Yang, H.J., Wang, W.Z., Liu, J.Q., Chen, L., 2022. Daytime warming triggers tree growth decline in the Northern Hemisphere. Glob. Chang. Biol. 28, 4832–4844. https://doi.org/10.1111/gcb.16238.

Thornley, J.H.M., 2011. Plant growth and respiration re-visited: maintenance respiration defined - it is an emergent property of, not a separate process within, the system - and why the respiration: photosynthesis ratio is conservative. Ann Bot-London 108, 1365–1380. https://doi.org/10.1093/aob/mcr238.

Thornley, J.H.M., Cannell, M.G.R., 2000. Modelling the components of plant respiration: Representation and realism. Ann Bot-London 85, 55–67. https://doi.org/10.1006/anbo.1999.0997.

Wang, W.Z., Jia, M., Wang, G.X., Zhu, W.Z., McDowell, N.G., 2017. Rapid warming forces contrasting growth trends of subalpine fir (*Abies fabri*) at higher-and lower-elevations in the eastern Tibetan Plateau. Forest Ecol Manag 402, 135–144. https://doi.org/10.1016/j.foreco.2017.07.043.

West, G.B., Brown, J.H., Enquist, B.J., 1999. A general model for the structure and allometry of plant vascular systems. Nature 400, 664–667. https://doi.org/10.1038/23251.

Xu, Z.F., Wan, C.A., Xiong, P., Tang, Z., Hu, R., Cao, G., Liu, Q., 2010. Initial responses of soil $CO_2$ efflux and C, N pools to experimental warming in two contrasting forest ecosystems, Eastern Tibetan Plateau, China. Plant and Soil 336, 183–195. https://doi.org/10.1007/s11104-010-0461-8.

Yu, D.P., Liu, J.Q., Lewis, B.J., Li, Z., Zhou, W.M., Fang, X.M., Wei, Y.W., Jiang, S.W., Dai, L.M., 2013. Spatial variation and temporal instability in the climate-growth relationship of Korean pine in the Changbai Mountain region of Northeast China. Forest Ecol Manag 300, 96–105. https://doi.org/10.1016/j.foreco.2012.06.032.

Zhang, C.L., Li, Q., Shen, Y.P., Zhou, N., Wang, X.S., Li, J., Jia, W.R., 2018. Monitoring of aeolian desertification on the Qinghai-Tibet Plateau from the 1970s to 2015 using Landsat images. Sci. Total Environ. 619, 1648–1659. https://doi.org/10.1016/j.scitotenv.2017.10.137.

Zhang, H., Shao, X.M., Zhang, Y., 2015. Which climatic factors limit radial growth of Qilian juniper at the upper treeline on the northeastern Tibetan Plateau? J. Geog. Sci. 25, 1173–1182. https://doi.org/10.1007/s11442-015-1226-3.